Geochemistry, Geophysics, Geosystems

RESEARCH ARTICLE
10.1029/2019GC008232

Deep Water Cycling and Sea Level Change Since the Breakup of Pangea

Krister S. Karlsen[1], **Clinton P. Conrad**[1], **and Valentina Magni**[1]

[1]Centre for Earth Evolution and Dynamics, University of Oslo, Oslo, Norway

Key Points:
- An imbalance between water fluxes into the mantle at trenches and out of the mantle at ridges may have changed sea level since Pangea time
- We estimate ocean mass change from tectonic reconstructions using parameterizations of subduction water flux based on slab age and velocity
- Faster slabs during Pangea breakup transported extra water to the mantle, contributing to a sea level drop of up to ~130 m since 230 Ma

Correspondence to:
K. S. Karlsen,
k.s.karlsen@geo.uio.no

Citation:
Karlsen, K. S., Conrad, C. P., & Magni, V. (2019). Deep water cycling and sea level change since the breakup of Pangea. *Geochemistry, Geophysics, Geosystems*, *20*, 2919–2935. https://doi.org/10.1029/2019GC008232

Received 29 JAN 2019
Accepted 11 MAY 2019
Accepted article online 17 MAY 2019
Published online 24 JUN 2019

Abstract First-order variations in sea level exhibit amplitudes of ~200 m over periods that coincide with those of supercontinental cycles (~300–500 Myr). Proposed mechanisms for this sea level change include processes that change the container volume of the ocean basins and the relative elevation of continents. Here we investigate how unbalanced rates of water exchange between Earth's surface and mantle interior, resulting from fluctuations in tectonic rates, can cause sea level changes. Previous modeling studies of subduction water fluxes suggest that the amount of water that reaches sub-arc depths is well correlated with the velocity and age of the subducting plate. We use these models to calibrate a parameterization of the deep subduction water flux, which we together with a parameterization of mid-ocean ridge outgassing, then apply to reconstructions of Earth's tectonic history. This allows us to estimate the global water fluxes between the oceans and mantle for the past 230 Myr and compute the associated sea level change. Our model suggests that a sea level drop of up to 130 m is possible over this period and that it was partly caused by the ~150Ma rift pulse that opened the Atlantic and forced rapid subduction of old oceanic lithosphere. This indicates that deep water cycling may be one of the more important sea level changing mechanisms on supercontinental time scales and provides a more complete picture of the dynamic interplay between tectonics and sea level change.

1. Introduction

Liquid water on Earth's surface constitutes the blue fingerprint of our planet within the solar system and is a key characteristic that is considered essential for life (Kasting & Catling, 2003) and the operation of plate tectonics (Korenaga, 2013). However, surface water amounts to only a fraction of Earth's total water content, as both hydrous and nominally anhydrous minerals store water within Earth's mantle (Hirschmann, 2006; Hirschmann & Kohlstedt, 2012). Recent estimates of Earth's mantle water content range from about one present-day ocean mass (OM = $1.4 \cdot 10^{21}$ kg; Bodnar et al., 2013) to seven OM (Nestola & Smyth, 2016). Even more extraordinary, water is not stationary in either of these reservoirs but is recycled between them. Through subduction of sediments and hydrated oceanic lithosphere, water is transported from the oceans into the mantle (*regassing*) and returned to the exosphere (here oceans and atmosphere) through volcanism (*degassing*). For most of Earth history (Korenaga et al., 2017) and for the present day (Peslier et al., 2017), the regassing flux is thought to be larger than the degassing flux. Therefore, ocean water mass should be time dependent, not only due to variations in landbound water storage (ice and groundwater) but also due to imbalanced deep water cycling.

Sedimentary stratigraphy provides evidence (fairly consistent for the last 250 Myr, less so for deeper time) for global-scale cycles of sea level change throughout the Phanerozoic that coincide well with the supercontinental cycle (see, e.g., Nance et al., 2014; Figure 1a). The proposed mechanisms for these sea level variations include processes that change ocean basin container volume (changes to ocean area, the volume of spreading ridges, dynamic topography, and the emplacement or removal of sedimentary and volcanic materials) and those that affect the thermal elevation of continents, for example, by trapping of heat beneath them (Conrad & Husson, 2009; Worsley et al., 1984). Imbalanced exchange of water between the Earth's oceans and its mantle can also change sea level (Ito et al., 1983; Parai & Mukhopadhyay, 2012), but the time history and amplitude of this imbalance remains poorly understood (Conrad, 2013; Cloetingh & Haq, 2015).

Here we investigate deep water recycling as an additional sea level-changing mechanism operating on the time scales of supercontinent cycles. Plate reconstruction models provide evidence for significant changes to the tectonics of ocean basins (Figures 1b–1e), and the slabs that descend from them (Figures 1h and 1i)

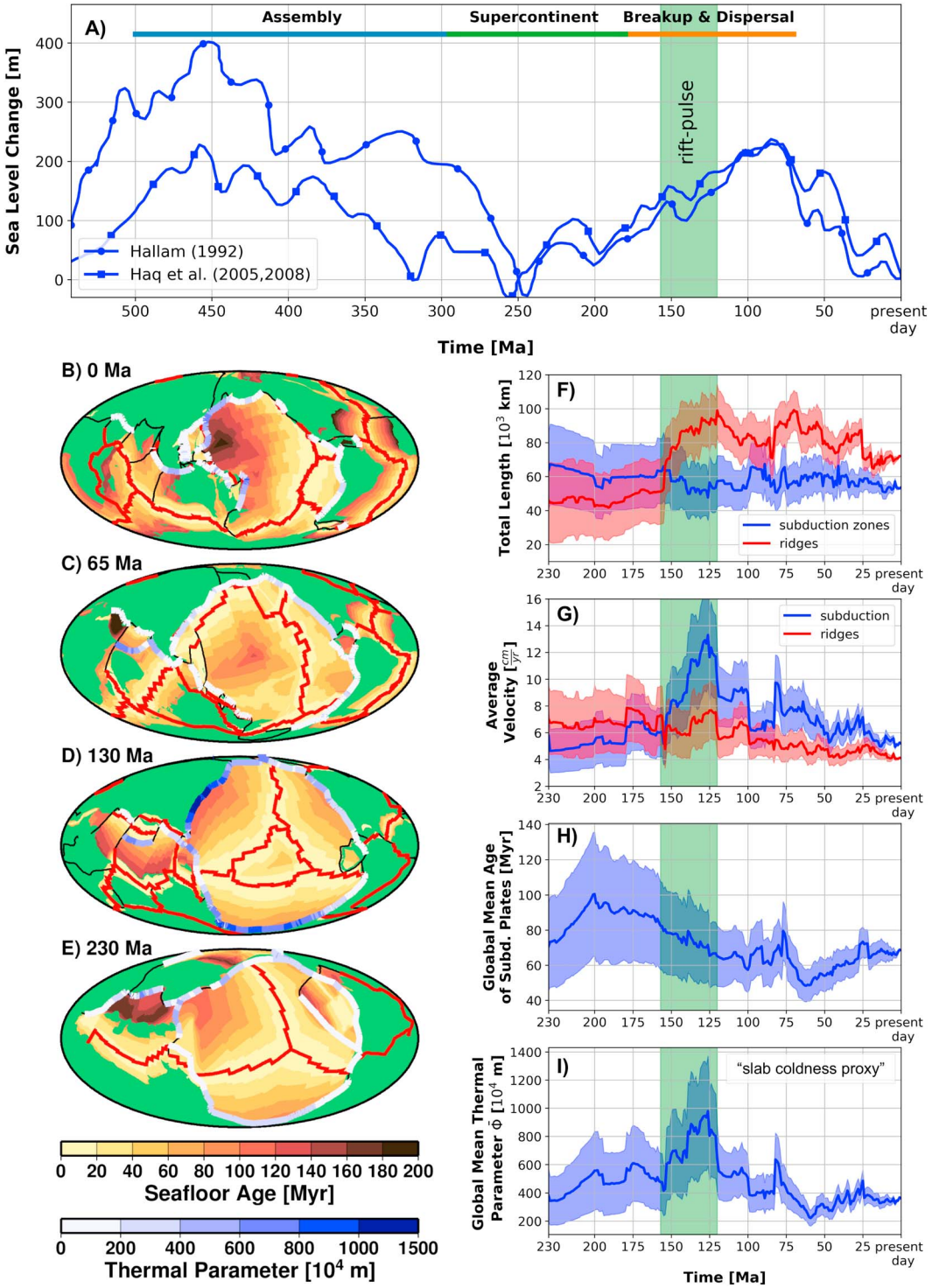

Figure 1. Phanerozoic sea level (a) (Hallam, 1992; Haq et al., 2005; Haq & Schutter, 2008) shows variations that correlate with supercontinental phases of Pangea (markers based on Cogné & Humler, 2008, and Li & Zhong, 2009). Reconstructions of past seafloor configurations (b–e) back to 230 Ma (Müller et al., 2016) indicate temporal changes in length (f) and spreading rate (g) of the ridge system, and in the length (f), convergence velocity (g), age (h), and thermal parameter (i) of subduction zones. The rift pulse that led to the breakup of Pangea between 160 and 120 Ma is highlighted in green (a and f–i). Shaded envelopes (red and blue, f–i) represent one standard deviation of the considered variations in the tectonic parameters (see Appendix A).

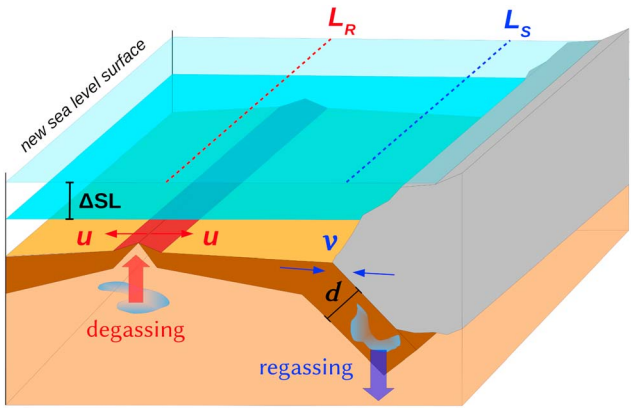

Figure 2. A simplified illustration of the deep water cycling and sea level box model, showing one subduction zone segment and one ridge segment, which are described by model parameters: subduction zone length L_S, ridge length L_R, full spreading velocity u, full convergence velocity v, and subducting plate thickness d. We use values for these parameters taken from the Müller et al. (2016) tectonic reconstruction. The sea level change associated with deep water cycling is denoted by ΔSL.

since Pangean times. Such variations have led to global changes in plate boundary lengths and rates associated with seafloor spreading and subduction during the last supercontinental cycle (Figures 1f–1g). As an example, during the breakup phase of Pangea and the opening of the Atlantic ocean, the global mid-ocean ridge system doubled in length. The tectonic record (e.g., Müller et al., 2016; Matthews et al., 2016) suggests that this rift pulse was compensated by rapid subduction of old oceanic lithosphere (Figures 1f and 1g) around the margins of the ancient supercontinent. These constraints are critical for understanding water exchange between the oceans and Earth's interior because ridges and subduction zones represent the main gateways for deep water fluxes (Kelemen & Manning, 2015; Keller et al., 2017).

Parameterized models of whole mantle convection have been used to study deep water recycling over the history of the Earth (Crowley et al., 2011; Korenaga, 2011; McGovern & Schubert, 1989; Sandu et al., 2011). These models provide valuable insight into the gross hydrological evolution of an Earth-like planet but are unable to capture changes on the 10^1–10^2 Myr time scales over which drastic variations in tectonic setting can occur (Figures 1b–1i). Here we propose a new and improved parameterization of the subduction water flux and apply it to the tectonic reconstructions of Müller et al. (2016). This allows us to infer time-dependent rates for the exchange of water between Earth's oceans and the mantle over the last 230 Myr and enables us to better understand the interaction between tectonics, deep water cycling, and sea level change.

2. Methods

2.1. Computing Deep Water Fluxes and Sea Level Change

The deep water cycle, and the evolution of Earth's interior and surface water reservoirs, can be constrained by combining flux estimates at the main gateways (ridges and trenches). However, determining the magnitudes of these fluxes is far from trivial; the amount of water that can be transported by a slab into the deep mantle depends on factors such as mantle temperature, slab lithology, slab age, initial water content, and subduction velocity. Of the slab's initial water content, only a small fraction can be carried beyond the arc and recycled into the deeper mantle, while the rest is released to the arc via a series of metamorphic reactions. The timing of dehydration, and the mass of water that can be retained at a certain depth have been studied using thermopetrological models (Hacker, 2008; Rüpke et al., 2004; Syracuse et al., 2010; van Keken et al., 2011). These studies find that the amount of water retained at larger depths (>200 km) is well correlated with both the age and velocity of the subducting plate (Magni et al., 2014), which suggests that the subduction water flux can be parameterized in terms of these quantities. This is mainly because old and fast slabs maintain a colder interior for longer compared to young and slow ones and, thus, have the potential to bring water to depths at which high pressure hydrous minerals (such as phase A) are stable. Moreover, the cold geotherm of an old plate allows for deep thermal cracking (Korenaga, 2007, 2017) and for deep normal faults at trenches (Faccenda et al., 2012; Ranero & Sallares, 2004) that can enhance deep hydration of the lithospheric mantle in old plates.

For a subduction zone segment (Figure 2) with length L_S, convergence velocity v, plate thickness d, and density ρ, the rate of mass transport of oceanic plate into the mantle is given by $\rho v d L_S$ (kg/year). The rate of water transport into the mantle is then given by $\alpha \rho v d L_S$, where α is the nondimensional *regassing factor* that relates to the plate's initial bulk water content. However, of the total initial water content, only a small fraction ϵ can be carried deep into the mantle because of a significant loss to arc volcanism. We then estimate the deep mantle water flux as $\alpha \epsilon \rho v d L_S$, where we compute the plate thickness from the plate age τ using the half-space cooling model (Parsons & Sclater, 1977) while enforcing a maximum thickness of 100 km, achieved at $\tau \sim 80$ Ma (Sclater et al., 1980).

Following previous studies (Garrels, 1983; Hirschmann, 2018; Marty & Tolstikhin, 1998; McGovern & Schubert, 1989), we assume that the degassing rate at mid-ocean ridges is proportional to the sea floor production rate. This is a reasonable assumption if the global mean upper mantle temperature and water

content does not change significantly over the period of interest (last 230 Myr). We thus compute degassing for a ridge segment of length L_R according to $\gamma \rho u h L_R$, where u is the full spreading velocity, h is the average thickness of produced crust, and γ is the *degassing factor*. Physically, the degassing factor can be interpreted as the product of the concentration of water within the melt and the fraction of that water that degasses (rather than remaining bound in the oceanic crust as it solidifies).

To estimate regassing and degassing rates back in time, we use the tectonic reconstruction model of Müller et al. (2016), which provides information about plate motions and plate boundary evolution since 230 Ma. In order to avoid including inactive plate boundaries (i.e., boundary segments classified as ridges and subduction zones that are not diverging or converging), we apply a threshold of 0.2 cm/year for which a plate boundary must either diverge or converge to be counted as a ridge or a subduction zone. Although this filtering affects the total length of the ridge and subduction zone systems (temporal variations are shown in Figure 1f), it does not significantly affect the total rate of area creation or destruction. At each point in time, we obtain from plate boundary segments classified as *subduction zones*: segment length L_S, convergence velocity v, and subducting plate age τ. For *mid-ocean ridge* boundaries we collect segment length L_R and the full spreading rate u. The length-weighted average of these quantities for the past 230 Myr (Figures 1f–1i) shows variations that should produce temporal variations in degassing and regassing rates. We compute global deep water fluxes for a given time $t \in [0, 230]$ Ma by summing over all segments:

$$\text{Regassing}: \quad R(t) = \sum_i \alpha \epsilon \rho d(\tau_i) v_i L_{Si}, \tag{1}$$

$$\text{Degassing}: \quad D(t) = \sum_j \gamma \rho h u_j L_{Rj}. \tag{2}$$

Here i sums over all subduction segments and j sums over all ridge segments. For the practical purposes of this study, α and γ serve as free parameters that are determined by assuming present-day rates of regassing $R(0)$ and degassing $D(0)$. This allows us to investigate a wide range of present-day degassing and regassing fluxes (associated with pairs of α and γ values), and their impact on sea level history.

Given time-dependent rates of regassing $R(t)$ and degassing $D(t)$, the component of sea level change associated with imbalanced deep water recycling can be computed as

$$\Delta \text{SL}(t) = -\frac{\lambda}{\rho_w A_o} \int_0^t R(t) - D(t)\, \mathrm{d}t. \tag{3}$$

where ρ_w is the density of water, A_o is the ocean area, and $\lambda = (\rho - \rho_w)/\rho \approx 0.7$ is a correction factor for isostatic adjustment of the oceanic lithosphere as sea level changes (Pitman, 1978).

2.2. Uncertainty in Tectonic Reconstructions

The plate tectonic reconstructions of Müller et al. (2016) do not include measures of uncertainty. However, since the ocean floor acts as a recorder of plate motion history, uncertainty is bound to increase backward in time as an increasingly larger fraction of Earth's present-day surface is missing. This fraction is commonly referred to as the "world uncertainty" and is a proxy for the uncertainty in any plate motion history model (Domeier & Torsvik, 2017). To account for this time-dependent uncertainty, we explore the sensitivity of our model results to variations in the tectonic parameters (L_S, v_S, L_R, v_R, and τ) that scale with the world uncertainty. This is accomplished using Monte Carlo methods, where each model is run 10^4 times (after which the model output distributions have converged) with the tectonic parameters drawn from the assumed probability distribution. This enables us to infer upper and lower bounds on our model results. One standard deviation of the considered variation in the tectonic parameters is shown in Figures 1f–1h. For a more detailed description of the Monte Carlo sampling, see Appendix A.

2.3. Parameterization of Slab Dehydration

Parameterizations of regassing have been used in coupled thermal and water cycling models to study Earth-like planetary evolution (Crowley et al., 2011; McGovern & Schubert, 1989; Sandu et al., 2011). However, these parameterizations have been applied to global averages of plate movement and are not well suited to predict water fluxes at individual subduction zones (Figure 3d). An explanation for this can be provided by the fact that slab dehydration patterns can vary greatly, depending on the thermal structure of individual subduction zones (van Keken et al., 2011), while thermal evolution models naturally assume a global average parameter ϵ (that is also constant through time) that accounts for dehydration.

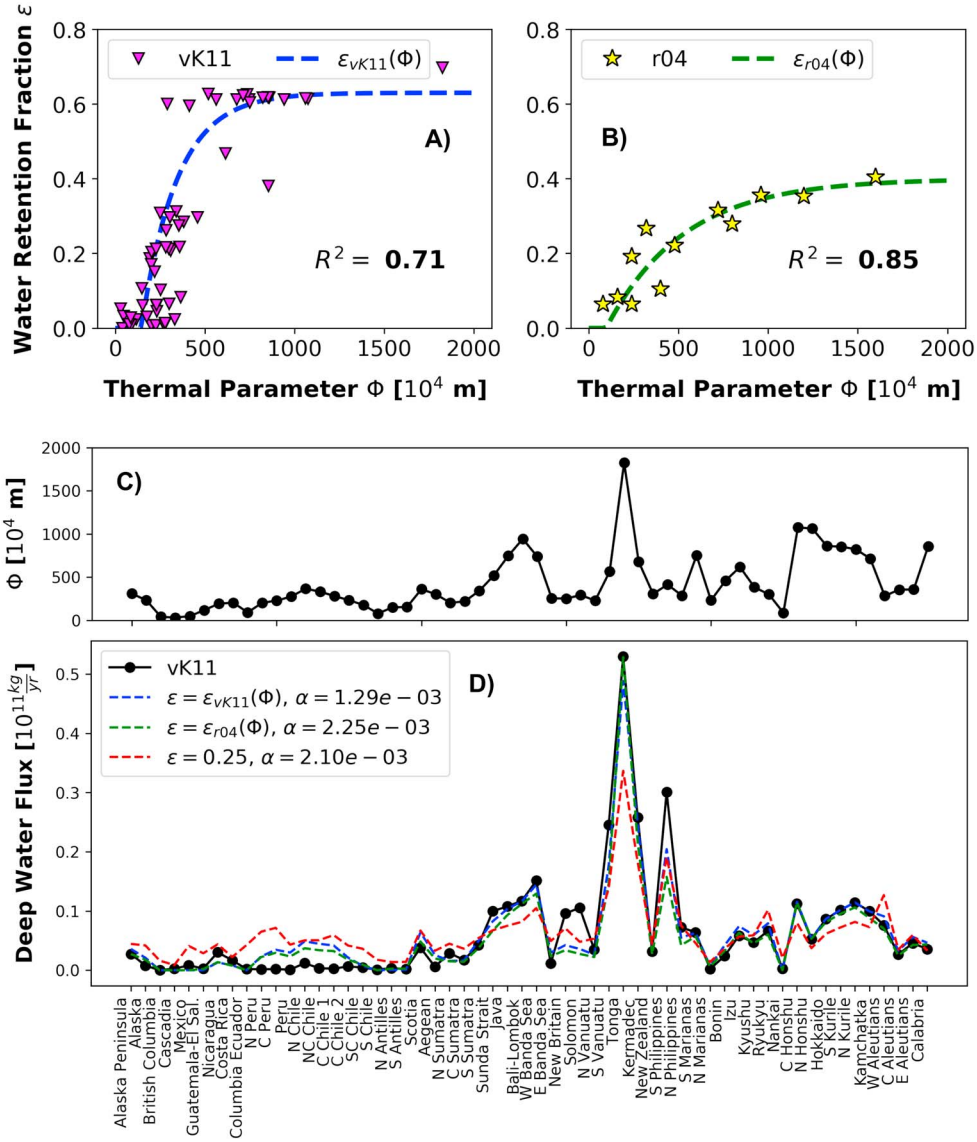

Figure 3. Relative slab water retention ϵ as a function of the slab's thermal parameter for two independent studies, vK11 = van Keken et al. (2011) (a) and r04 = Rüpke et al. (2004) (b), and a functional (equation (4); see Table 1 for coefficients) fit to these reported values. The coefficient of determination R^2 indicates how much of the variance that can be explained by the paramterization. Present-day subduction zones' thermal parameter (c), and a comparison between their estimated deep water fluxes (d) based on the reported values (black dots) of van Keken et al. (2011; Table 1, serpentinization 230 km) and our regassing parameterization (1) using a constant water retention fraction ϵ (red), the fit to vK11 (blue), and the fit to r04 (green). Values for Φ and ϵ for vK11 (a) are computed based on values from "Table 1: serpentinization," while values for r04 (b) are from "Figures 7a and 7e" in their respective publications.

The thermal structure of subduction zones is controlled by the descending oceanic plate's initial temperature profile and the kinematics of subduction. This relationship is often described using the *thermal parameter* Φ, which we here define as the subduction convergence velocity times the plate age. Other definitions may include dip angle (Kirby et al., 1996), but it has recently been suggested that the dip angle only exhibits second-order control on the slab geotherms compared to the effects of plate age and velocity (Maunder et al., 2019). Data from tectonic reconstructions (Müller et al., 2016) show that the thermal parameter of subduction zones has varied dramatically through time (Figure 1i). Therefore, to better predict the mantle water flux for individual subduction zones in the past, we propose an expression for the slab's ability to retain water as function of its thermal parameter, that is, $\epsilon(\Phi)$.

Table 1
Model parameters (constants), input iarameters taken from tectonic reconstructions (Müller et al., 2016), coefficients used in the water retention paramterizations, and scaling parameters used for the three deep water cycling cases considered in Figure 4

Description	Symbol	Value		
Model parameters				
Upper mantle density	ρ	3,200 kg/m^3		
Water density	ρ_w	1,000 kg/m^3		
Ocean area	A_o	$3.62 \cdot 10^{14}$ m^2		
Mean oceanic crust thickness	h	7.0 km		
Isostatic correction factor	λ	0.7		
Input parameters from tectonic reconstructions				
Length of subduction segment i	L_{Si}	varies with time and segment		
Length of ridge segment j	L_{Rj}	varies with time and segment		
Convergence velocity for segment i	v_i	varies with time and segment		
Spreading velocity for segment j	u_j	varies with time and segment		
Age of subducting plate segment i	τ_i	varies with time and segment		
Constants in water retention function fit				
Paramterization		a	b	c
vK11		−0.67	1.3	0.005
r04		−0.1	0.5	0.0023
Scaling parameters used for special cases				
Regassing parameterization using ϵ_{vK11}				
Case	α	γ	R(0)	D(0)
Long-term balance (LB)	5.40e−4	3.15e−3	$1.5 \cdot 10^{11}$ kg/year	$2.0 \cdot 10^{11}$ kg/year
Present-day balance (PB)	7.00e−4	3.15e−3	$2.0 \cdot 10^{11}$ kg/year	$2.0 \cdot 10^{11}$ kg/year
Regassing dominated (RD)	1.18e−3	3.15e−3	$3.5 \cdot 10^{11}$ kg/year	$2.0 \cdot 10^{11}$ kg/year
Regassing parameterization using ϵ_{r04}				
Long-term balance (LB)	1.07e−3	3.15e−3	$1.5 \cdot 10^{11}$ kg/year	$2.0 \cdot 10^{11}$ kg/year
Present-day balance (PB)	1.33e−3	3.15e−3	$2.0 \cdot 10^{11}$ kg/year	$2.0 \cdot 10^{11}$ kg/year
Regassing dominated (RD)	2.28e−3	3.15e−3	$3.5 \cdot 10^{11}$ kg/year	$2.0 \cdot 10^{11}$ kg/year

To obtain a first-order understanding of how slab water retention depends on the thermal parameter, we plot the fraction of water retained at >200-km depth based on results from two independent studies (Figures 3a and 3b). The overall trends are similar in the sense that the relative water retention increases with the thermal parameter until a saturation threshold is reached. They do however, differ in the magnitude of this saturation point, where results of van Keken et al. (2011) suggest that slabs can retain ∼60% of their initial water content, while Rüpke et al. (2004) suggest that ∼40% of the water that can be retained. We find that an exponential function with a negative exponent is suitable to describe a subducting plate's relative water retention ϵ as a function of its thermal parameter Φ:

$$\epsilon(\Phi) = \max\left(0, a + b(1 - e^{-c\,\Phi})\right). \tag{4}$$

The constants a, b, and c used to fit the two independent data sets are given in Table 1. Including this function in our model effectively modifies equation (1) by replacing ϵ with $\epsilon_{vK11}(\Phi_i)$ or $\epsilon_{r04}(\Phi_i)$, where $\Phi_i = v_i\tau_i$ and r04 and vK11 refer to the two different functional fits (defined by different values of a, b, and c; Table 1) shown in Figures 3a and 3b. Because the results reported by Rüpke et al. (2004) follow a clearer trend than those of van Keken et al. (2011), the functional fit (equation (4)) to the results of Rüpke et al. (2004) yield a higher coefficient of determination ($R^2 = 0.85$), meaning that 85% of the variance in the relative water retention ϵ can be explained by our parameterization through the thermal parameter Φ. On the other hand, the fit to the results of van Keken et al. (2011) can explain 71% of the variance (Figures 3a and 3b).

The most detailed study of water transport at individual subduction zones is van Keken et al. (2011), who estimated the H_2O flux for Earth's present-day subduction zones by combining finite element models for

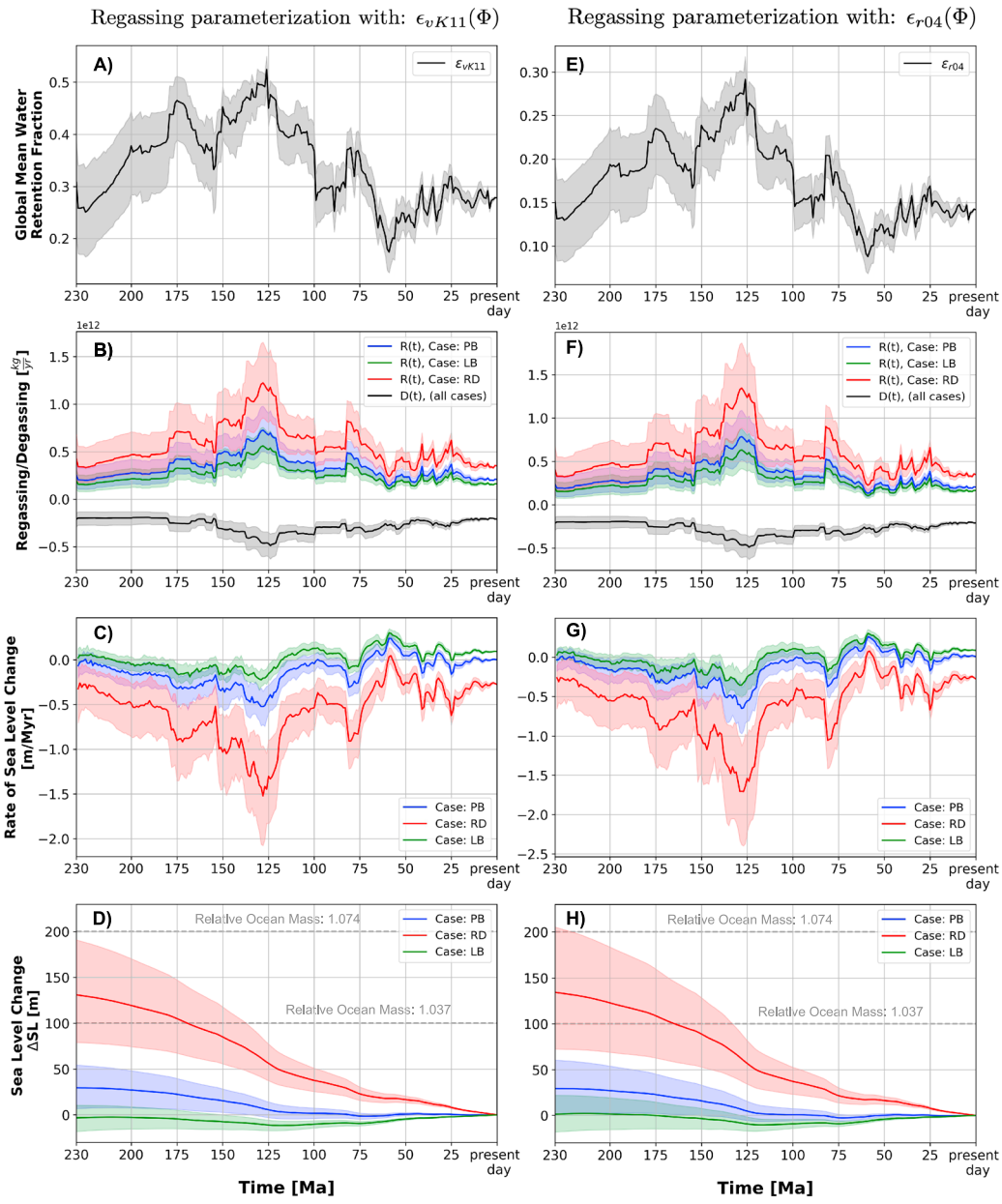

Figure 4. Tectonically inferred time history of deep water cycling and its associated ocean mass and sea level change for two different parameterizations of slab water retention (left and right columns correspond ϵ_{vK11} and ϵ_{r04}, respectively). Global mean water retention fractions $\bar{\epsilon}$ (a and e) and deep water flux rates (b and f) for three scenarios: regassing dominated (RD: red), present-day balance (PB: blue), and long-term balance (over the past 230 Myr; LB: green) are presented along with corresponding sea level changes (d and h) and their rates of change (c and g). Solid curves show the median of 10^4 Monte Carlo simulations, while the enveloping shaded areas represent the upper and lower quartiles of the distributions. The α and γ values used to produce these results can be found in Table 1 and a detailed description of the Monte Carlo methods is found in Appendix A.

each subduction zone with a petrological model that tracks water retention with depth. To see if including a dependence on the thermal parameter in the water retention (4) improves the parameterization of subduction water flux (1), we apply it to the present-day subduction zones and compare it to the published estimates of van Keken et al. (2011). We see that by using both ϵ_{vK11} and ϵ_{r04} in the parameterization (1), we can capture differences between individual subduction zones better than we can using a constant ϵ (Figure 3d). Conversely, the parameterization (1) with constant water retention is not able to fit subduction zones with a high thermal parameter, while at the same time fit subduction zones with a low thermal parameter

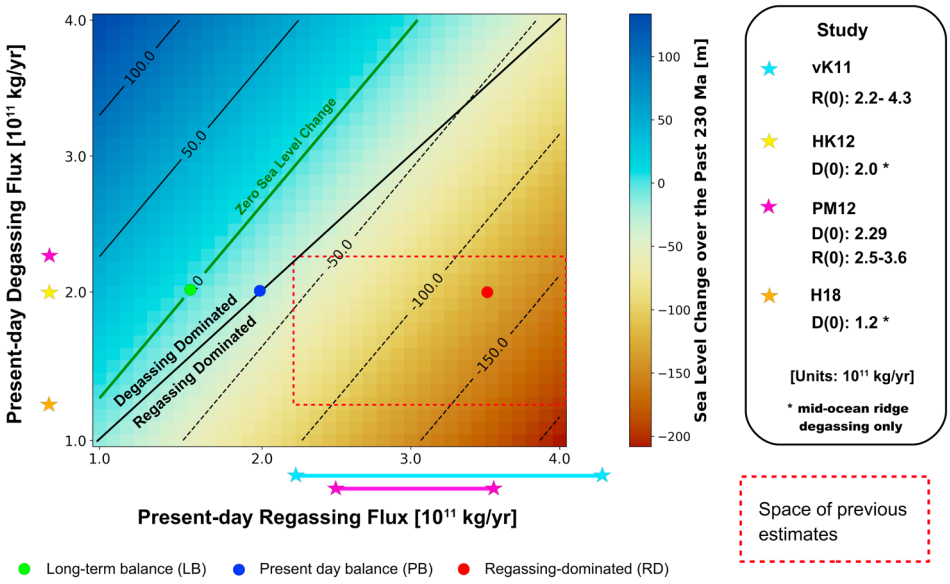

Figure 5. Net sea level change since 230 Ma, for combinations of present-day regassing and degassing rates between 1.0–4.0 $\cdot 10^{11}$kg/year H_2O. The green line marks zero sea level change over this period (including case LB), and the black line shows a present-day balance between regassing and degassing (including case PB). The corresponding sea level curves (which are nearly identical for ϵ_{vK11} and ϵ_{r04}) in Figures 4d and 4h are indicated by circle markers. Stars indicate previous estimates of present deep water fluxes (vK11, van Keken et al., 2011; HK12, Hirschmann & Kohlstedt, 2012; PM12, Parai & Mukhopadhyay, 2012; and H18, Hirschmann, 2018) and define the space of previous estimates (dashed red line).

(Figures 3c and 3d). As an example, using a constant water retention underestimates the deep water flux at the Tonga trench while overestimating almost all other fluxes. Therefore, applying the same constant ϵ to times during which the global mean thermal parameter was significantly higher (Figure 1i) would cause us to underestimate the global subduction water flux. Another improvement is that the functional form (4) allows for complete dehydration of slabs, which is believed to be the case for young plates subducting slowly (van Keken et al., 2011). It is also worth noting that despite having significantly different saturation points in terms of the relative water retention, the two different models (using ϵ_{vK11} and ϵ_{r04} in equation (1)) predict very similar magnitudes for the deep water fluxes, but they require different values of the free parameter α.

3. Results

By applying our parameterizations for the regassing (equations (1) and (4)) and degassing (equation (2)) fluxes to the tectonic reconstructions of Müller et al. (2016), we investigate temporal changes in regassing efficiency (Figures 4a and 4e), the magnitude of the deep water fluxes (Figures 4b and 4f) and their related sea level change (Figures 4c and 4d, and 4g and 4h).

Because Earth's current deep water flux rates are uncertain (a recent review of Peslier et al., 2017, suggests ~50% uncertainty), we explore a range of scenarios for deep water recycling associated with a range of present-day degassing and regassing rates. By tracking imbalances in these rates, we can compute the change in ocean mass and estimate sea level change (equation (3)) over the last 230 Myr. To understand the time-dependent coupling between deep water cycling and sea level change, we study three scenarios that we find to be particularly illustrating in detail; a *present-day balance* (PB) between regassing and degassing, a *long-term balance* (LB) since 230 Ma, and a *regassing-dominated* (RD) case that assumes a significant net flux of water into the mantle for the present day. These three cases are constructed by fixing the degassing parameter γ to produce a reasonable present-day degassing rate, that is, $2.0 \cdot 10^{11}$ kg/year (Hirschmann & Kohlstedt, 2012; Parai & Mukhopadhyay, 2012), and then finding the regassing parameter value α that satisfies the constraint for the given scenario (equations (5)–(7)). For the regassing-dominated case, we chose an α value that corresponds to the estimated subduction water flux of van Keken et al. (2011), which is $3.5 \cdot 10^{11}$ kg/year. All these pairs of α and γ values can be found in Table 1. The three cases can be expressed mathematically as

$$\text{Present-day balance:} \quad R(0) = D(0) = 2.0 \cdot 10^{11} \text{ kg/year} \tag{5}$$

$$\text{Long-term balance:} \quad \int_0^{230\ \text{Ma}} R(t) - D(t) \quad \mathrm{d}t = 0 \tag{6}$$

$$\text{Regassing dominated:} \quad R(0) = 3.5 \cdot 10^{11}\ \text{kg/year},\ D(0) = 2.0 \cdot 10^{11}\ \text{kg/year} \tag{7}$$

To further investigate the link between present-day deep water fluxes and past sea level change, we compute regassing, degassing, and sea level history for a range of combinations of α and γ values, corresponding to present-day regassing and degassing rates in the interval 1.0–4.0 $\cdot 10^{11}$ kg/year. These results (Figure 5) show the net sea level change since 230 Ma, with a black diagonal line indicating the transition between a degassing- and a regassing-dominated present day. A green line marks the combination of present-day deep water flux rates that would cause zero net sea level change since 230 Ma. The three circle markers show where the highlighted cases (PB, LB, and RD) plot in the parameter space. Finally, to link the estimated deep water fluxes to specific tectonic events we show maps of reconstructed subduction water fluxes for past times, which illustrate the regassing distribution between individual subduction zones (Figure 6).

Because we investigate variations in the tectonic input parameters (Figures 1f–1h) to our model through Monte Carlo sampling, the resulting global mean water retention histories (Figures 4a and 4e), water fluxes (Figures 4b and 4f), rates of sea level change (Figures 4c and 4g), and sea level and ocean mass changes (Figures 4d and 4g) are probability distributions (rather than single curves). These results are presented in Figure 4 as preferred estimates (defined by the median, solid curves) with upper and lower bounds (shaded areas) defined as the median of the upper half of the distribution and the median of the lower half of the distribution. These bounds are commonly referred to as *upper quartile* and *lower quartile*.

3.1. Regassing Efficiency Through Time

The global regassing flux directly depends on the rate at which seafloor area is consumed at subduction zones (1). To preserve seafloor area, this rate is approximately equal to the rate at which seafloor is created at ridges, which directly impacts the degassing rate (2). Thus, we expect the net degassing and regassing fluxes to exhibit proportional variations during periods of faster or slower plate creation and destruction. However, the regassing flux also depends on subducting plate age through the thickness d and ability to retain water ϵ, both of which have varied with time differently than the seafloor area destruction rate (Figures 1f–1h). Additionally, since the slab water retention also depends on the plate velocity (Magni et al., 2014; Rüpke et al., 2004; van Keken et al., 2011), the deep subduction water flux is nonlinear in plate velocity as well as age. Thus the rates of regassing and degassing depend on the tectonic record in different ways, which leads to time variations in the net flux of water into or out of the mantle.

For the present day, our two different models predict that slabs on average retain about 14–27% of their initial water content (Figures 4a and 4e). Here the lower estimate represents the paramterization of relative water retention based on the results of Rüpke et al. (2004), while the upper estimate corresponds to the paramterization motivated by van Keken et al. (2011). For comparison, recently published estimates include 26% (Magni et al., 2014) and 33% (van Keken et al., 2011). We note that despite giving significantly different values for water retention, the two models (ϵ_{vK11} and ϵ_{r04}) follow similar trends (Figures 4a and 4e) and yield nearly identical results in terms of deep water fluxes (Figures 4b and 4f) and associated sea level change (Figures 4d and 4h). Although they require different values of α, see Table 1. Our application of these models to the tectonic record suggests that today's fraction is relatively low within the last 230 Myr and that ϵ likely have been higher in the past. The current period of strong slab dehydration is caused by the combination of slow convergence velocities at subduction zones and moderately low subducting plate ages (Figures 1g and 1h), which together diminish the global average thermal parameter (Figure 1i).

The most prominent peak in average plate water retention (Figures 4a and 4e) is related to the major rift pulse around 150 Ma, associated with the opening of the South Atlantic Ocean (Figures 1 and 6). During this time, the total length of the ridge system approximately doubled, while the length of the subduction zone system actually dropped (Figure 1f). This caused a dramatic increase (well above a factor of 2) in the convergence velocity at the active trenches (Figure 1g). As old and hydrated oceanic lithosphere was rapidly forced into the mantle by the new, massive ridge system, the average age of subducting plates dropped about 20 Myr over this ~35-Myr period (Figure 1h). Despite the gradual loss of old seafloor, the average thermal parameter for subduction zones also more than doubled during the rift pulse (Figure 1i). This period of

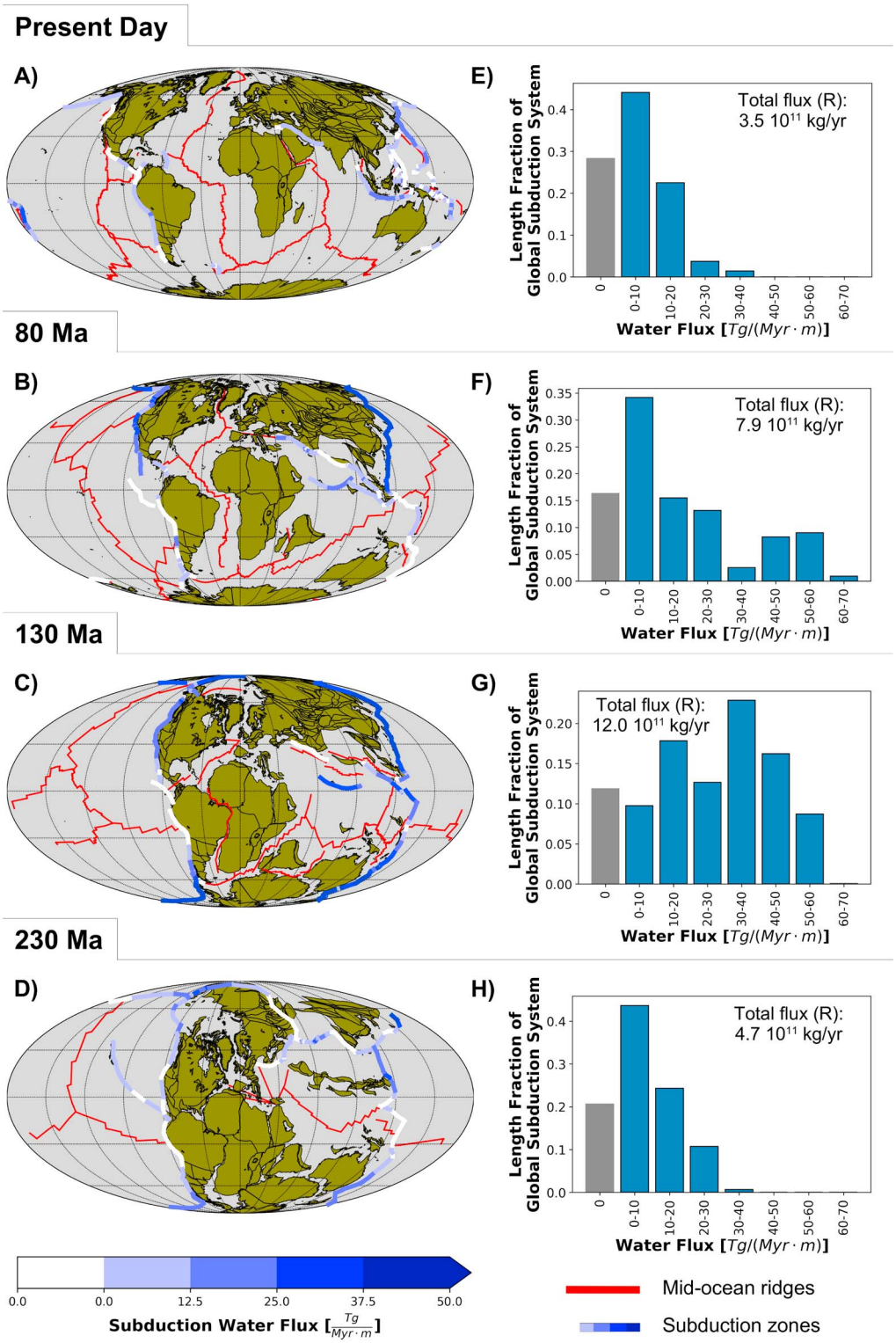

Figure 6. Reconstructed maps (a–d) based on Müller et al. (2016) showing ridges (red) and the subduction water flux (shades of blue) through time. Histograms (e–h) show the distribution of subduction zone segments according to how much water they transport into the deep mantle. The regassing estimates here correspond to the regassing-dominated case (nearly identical for ϵ_{vK11} and ϵ_{r04}), which assumes a present-day global subduction water flux comparable to that of van Keken et al. (2011).

anomalously rapid subduction allowed for a large fractions of water (on average about 30–50%) to be carried to sub-arc depths (Figures 4a and 4e).

3.2. Time-Dependence of the Deep Water Cycling

Our estimates of regassing and degassing history (Figures 4b and 4f) suggest that the deep water flux rates have remained fairly stable since the breakup phase of Pangea ended about 70 Myr ago. Thus, our model indicates that any net flux to or from the mantle (including zero net flux), and the associated rate of sea level change (Figures 4c and 4g), has been approximately constant since 70 Ma. This is because the average convergence velocity at subduction zones has steadily decreased over this time period (Figure 1g), while the mean age of subducting plates have steadily increased (Figure 1h), causing the thermal parameter (Figure 1i) and thus the global regassing efficiency (Figures 4a and 4e) to be approximately constant. It is worth noting that also prior to the dispersal of Pangea (before 180 Ma), our calculations suggest regassing and degassing to have been relatively stable. Three prominent peaks in regassing, (~175, 130, and 75 Ma) coincide with those of regassing efficiency $\bar{\epsilon}$ (Figures 4a and 4b, and 4e and 4f) and can be explained through their common occurrence at times with peaks in global mean values of subducting plate age and/or velocity (Figures 1g–1i). The maximum value of the largest regassing peak is about four times the present-day value, which is relatively low compared to last 230 Myr (Figures 4b and 4f). For the degassing flux, the maximum value occurs at the end of the rift pulse (~125 Ma) and is about 2.5 times as large as the present-day value.

Too see how the subduction water flux is distributed among different subduction zones through time (following the example of van Keken et al., 2011 , who did this for the present day), we show reconstructed maps with regassing flux estimates (Figure 6) based on our parameterization ($\epsilon_{\nu K11}$). We see that presently about 30% of subduction zones carry no water beyond the arc, while the rest have relatively low transport rates, most below 20 Tg/Myr/m (Figure 6e). On the other hand, right after the ~130 Ma rift pulse, the remnants of the ancient supercontinent was surrounded by subduction zones that transported more than 20-Tg/Myr/m water to the deep mantle (Figure 6g). Before the major rifting event, in late Pangean times (230 Ma, Figure 6h), we interestingly see that the distribution of subduction water flux was similar to that of the present day. These spatial and temporal variations in deep water fluxes may create a heterogeneous distribution of water in the mantle.

From the imbalanced regassing and degassing rates (Figures 4b and 4f), we compute the change in ocean mass over time, which we translate to sea level change through equation (3). Note that as several simplifying assumptions regarding ocean hypsometry go into this equation, our estimates in ocean mass change should be considered more robust than our sea level inferences. From the long-term balance scenario (LB; equation (6)), we interestingly see that the degassing flux must be about 33% larger than the regassing flux at the present day in order to not change sea level (or ocean mass) over the last 230 Myr. If regassing and degassing are currently in balance (PB; equation (5)), we expect a sea level drop of about 30 ± 25 m (~1% in ocean mass change), over the last 230 Myr, with most of the drop occurring between 230 and 120 Ma. The regassing-dominated case (RD, equation (7)) predicts an even larger sea level drop of 130 ± 50 m (~5% in ocean mass change) for the same period, which translates to an average net flux to the mantle of 2–4 $\cdot 10^{11}$ kg/year, or an ocean mass change of about 5%. The fastest rate of sea level change was about −1.5 ±0.5 m/Myr at about 130 Ma (Figures 4c and 4g).

4. Discussion

4.1. Amplitude of Sea Level Drop

Despite relatively high uncertainties tied to the present-day deep water fluxes, there seems to be consensus that there is a significant net flux of water into the mantle at the present day (e.g., Korenaga et al., 2017; Peslier et al., 2017); thus, we consider the present-day balance scenario to be conservative and the long-term balance to be unlikely (Figure 4), yet interesting cases to discuss. On the other hand, if there is a significant present-day net-flux of water into the mantle, as many studies suggest, the sea level drop caused by ocean-mantle water exchange may be as large as ~130 m (Figures 4 and 5). Although this scenario predicts past global subduction water fluxes that are much higher (4 times) than for the present day, the regassing flux distribution (Figure 6g) shows that the vast majority of subduction zones transported water into the deep mantle at rates lower than currently estimated for the Tonga trench, that is, 47.7 Tg/Myr/m by van Keken et al. (2011).

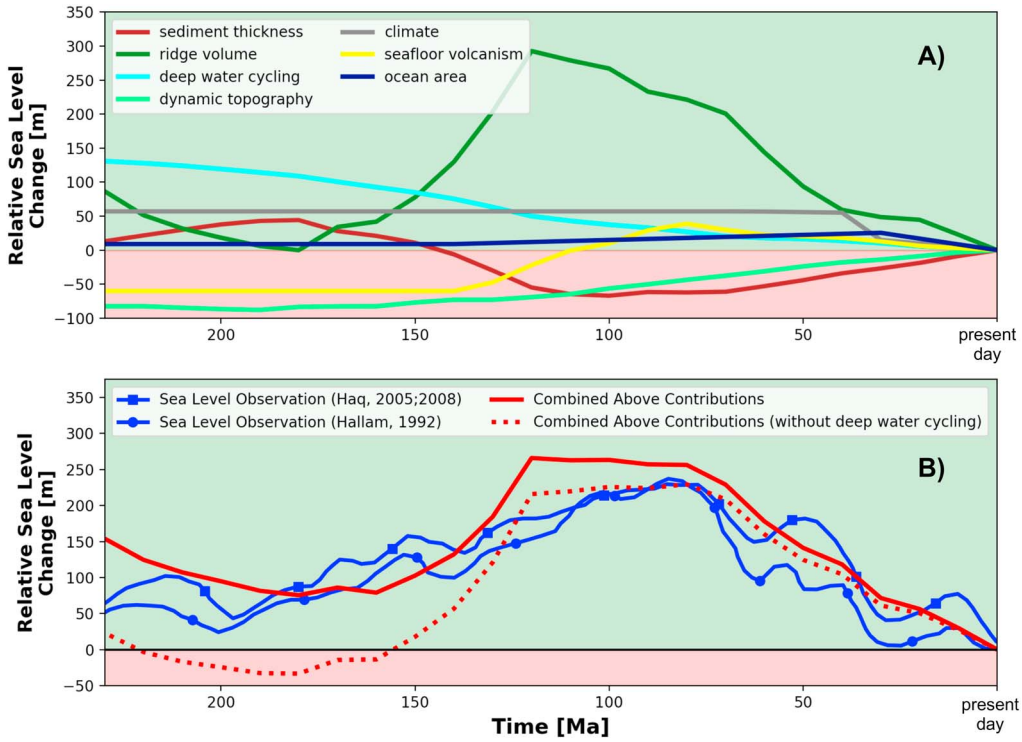

Figure 7. Sea level budget for the past 230 Myr. Estimates of the major sea level changing mechanisms (a) and their combined effect on sea level compared to observations (b) for the past 230 Myr. We calculate changes in ridge volume and sediment thickness by applying the Crosby and McKenzie (2009) age-depth relation and the Straume et al. (2019) age-latitude-sediment relation (respectively) to the Müller et al. (2016) age grids for the past 230 Myr. We computed the contribution from dynamic topography following Conrad (2013) but using the tectonic reconstruction of Conrad et al. (2013) to extend back to 230 Ma. We use Conrad (2013) estimates for the sea level contributions from changes to climate (melting of landbound ice and thermal expansion of seawater), seafloor volcanism, and ocean area back to 140 Ma, and, for lack of better information, assume that these contributions are constant for the period 250–140 Ma. We use the regassing-dominated (RD) case from this study for the deep water cycling component, and show the combined contributions both with (solid red line) and without (dashed red line) this contribution in (b).

New constraints on the subduction water flux were recently obtained through analysis of ocean-bottom seismic data (Cai et al., 2018). They find evidence for a partially serpentinized (2 wt% water) slab-mantle layer at the Mariana trench that is much thicker than previously assumed, indicating a greater extent of serpentenization in old slabs. These new constraints suggest that the water input to the Maraina trench should be 4.3 times higher than estimated by van Keken et al. (2011). Assuming that other old slabs have similar amounts of partially serpentinized mantle, Cai et al. (2018) estimate the global subduction water input to be 3 times higher than the previous estimates. This suggests that van Keken and colleagues' computation of the subduction water flux, and our regassing-dominated scenario (case RD), might be relatively conservative.

Our regassing-dominated scenario (Figure 4), which assumes a subduction water flux similar to that of van Keken et al. (2011), exhibits an average net flux of 2–4 $\cdot 10^{11}$ kg/year into the mantle during the past 230 Myr. Constraints based on an approximately constant continental freeboard since the Early Proterozoic (Korenaga et al., 2017) suggests that the net-flux to the mantle from the oceans must have been 3 and 4.5 $\cdot 10^{11}$ kg/year since ~2.5 Ga. This indicates that the estimates from our regassing-dominated present-day scenario largely overlap and are consistent with the suggested long-term drop in ocean water mass.

The above arguments and constraints suggest that deep water cycling caused a significant drop in ocean mass and should be considered as an important sea level changing mechanism for this period. This conclusion leads to a critical question: How much sea level drop can be added to the Mesozoic-Cenozoic sea level budget without violating the sea level record inferred from sedimentary stratigraphy (Hallam, 1992; Haq et al., 2005; Haq & Schutter, 2008)? Conrad (2013) added up estimated contributions for all the major sea level changing processes (changes in sediment thickness, ridge volume, dynamic topography, climate, ocean area, and the volume of structures formed by intraplate seafloor volcanism) for the past 140 Myr and compared it to the

sea level record. Here (Figure 7) we extend his analysis back to 230 Ma and include deep water cycling. We acknowledge that all these estimates, as well as the sea level observations themselves, are subject to very large uncertainties. That being said, we still consider this to be a useful exercise to place deep water cycling in the context of sea level history and other mechanisms. To highlight the effect of deep water cycling on the total sea level budget, we compare tallies with and without this effect to the observed sea level change (Figure 7b). We find that the deviation between observations and a sea level budget that includes deep water cycling is smaller than it is for the budget without deep water cycling over this period. This statement holds for both the sea level records we compare it to, indicating that there is room in the budget even for the largest of our sea level drop scenarios (case RD).

4.2. Ocean-Mantle Water Exchange over Supercontinent Cycles

A century of research has taken us from the fascination of Wegener's Pangea (Wegener, 1920), Earth's ancient supercontinent, to a realization that the formation and breakup of supercontinents is a general phenomenon of Earth history, beyond Pangea. There now seems to be acceptance that Earth has had at least five pre-Pangaen supercontinents at approximately 2.6, 2.0, 1.7, 1.1, and 0.6 Ga (Nance et al., 1986; Worsley et al., 1984, 1985). These supercontinental cycles are thought to have been associated with ocean-basin volume changes that changed sea level (Worsley et al., 1982, 1984). Here we have shown that such massive tectonic changes should also affect the deep water cycle, and thus induce major changes ocean water mass. Next, we will attempt, based on the limited tectonic record available, to generalize how the deep water fluxes induce sea level variations over supercontinent cycles.

The supercontinent cycle is traditionally divided into three phases: (1) *assembly*, (2) *supercontinent*, and (3) *breakup and dispersal*. It would perhaps be meaningful to add a fourth (4) *interstage*, which refers to a configuration of dispersed continents, in-between *breakup and dispersal* and a new *assembly* (corresponding to the present day). The supercontinent and the interstage configurations represent the most stable tectonic regimes; thus, we expect deep water cycling to be relatively stable as well during these phases. A similarity between these two phases is supported by our comparable predictions of the subduction water flux distributions during late Pangea and after its breakup and dispersal (Figures 6e and 6h), as well as fairly stable regassing and degassing fluxes during both of these periods (Figures 4b and 4f).

The breakup and dispersal of a supercontinent requires a massive rifting event that opens new oceans. The newly formed ridges must, in order to not significantly change the area of the ocean, be compensated by either (i) the creation of new subduction zones or (ii) an increase in convergence velocity at existing subduction zones. The most recent tectonic reconstructions (Matthews et al., 2016; Müller et al., 2016) suggest that the rift pulse during the last supercontinent cycle's dispersal phase (~150 Myr) was indeed compensated by rapid subduction of old oceanic lithosphere (Figures 1 and 6). Therefore, because of the strong velocity dependence of regassing, we expect an increased net-flux of water from the oceans into the mantle during supercontinental breakup and dispersal (Figure 4).

The final stage of supercontinent assembly involves the closing of an ocean basin through massive continent-continent collision that terminates subduction zones. Taking the present day as an example, the Atlantic Ocean has been growing at the expense of the Pacific where the major subduction zones are located. If this trend continues, the assembly of a supercontinent by closing the Pacific could potentially cause a significant drop in the subduction flux for a period of time, before new subduction zones develop (Silver & Behn, 2008). This should result in a temporary period of sea level rise. On the other hand, if the next supercontinent formed by closing the Atlantic, the majority of subduction zones located on the Pacific margins should endure, possibly without an accompanying period of sea level rise.

Generalizing rates of deep water transport over supercontinent cycles is challenging because no two cycles are likely to be identical, and the tectonic record currently provides information about only half of the last supercontinent cycle. However, it seems reasonable to infer that the deep water fluxes are most stable during supercontinental and interstage periods. The deep water cycling-induced sea level drop we expect to be associated with supertontinent breakup and dispersal, may be balanced to some extent by sea level rise during supercontinental assembly, although the extent of net degassing during assembly is difficult to constrain due lack of tectonic reconstructions for Pangean assembly. These expected sea level trends are generally consistent with our tectonically inferred predictions of water fluxes and sea level change (Figure 4) for the last phases of the last supercontinent cycle.

Over most of Earth's history, mantle cooling is thought to be associated with net regassing (Crowley et al., 2011; Korenaga, 2008, 2011), leading to a substantial loss of ocean mass and an accompanying sea level drop that may be partially obscured by secular evolution of continental buoyancy (Korenaga et al., 2017). The deep water cycling-induced sea level variations that we associate with the supercontinental cycle (described in the previous paragraph) may be superimposed on top of this long-term trend of net regassing, and/or may be the manifestation of the long-term trend itself. For example, repeated application of this sea level cycle would generate a long-term net regassing that is expected form thermal history models. However, if these variations are superimposed on a long-term trend of decreasing ocean mass, as predicted by previous studies (Crowley et al., 2011; Korenaga, 2011), we would likely also see a steady drop in sea level during interstage and supercontinentality. This scenario is reflected by the regassing-dominated case (Figure 4), where sea level drops both before and after the breakup of Pangea (~180–70 Ma), and does so even faster during the major rifting event (~150–120 Ma). These pulses of water entering the mantle during supercontinent breakup may thus represent an important part of Earth's long-term thermal and hydrological evolution.

4.3. Uncertainty of the Degassing History

We have assumed that degassing of water from the mantle occurs mainly at mid-ocean ridges and that the rate of this degassing is proportional to seafloor divergence rates. Two factors may complicate this assumption. First, intraplate degassing via volcanism at hot spots and large igneous provinces may be an important degassing contributor with a time dependence that differs from that of seafloor spreading. However, the range of degassing scenarios that we have explored (Figure 5) explores present-day mantle water output rates far beyond those of only mid-ocean ridges, which have been estimated for the present-day at about $1.2 \cdot 10^{11}$ kg/year (Hirschmann, 2018; Parai & Mukhopadhyay, 2012). Second, we assume that the melting zone beneath all the mid-ocean ridges contains the same amount of water. However, if water is heterogeneously distributed throughout the mantle (Hirschmann & Dasgupta, 2009), as we would expect given the heterogeneity associated with its entry into the mantle (Figure 6), we expect degassing along the ridge system to reflect these variations in the mantle water distribution. This is certainly important for estimating the degassing flux along certain ridge segments, but may not be as important for the global ridge flux since it is likely to average out across the entire ridge system.

5. Conclusions

The transport of surface water into deep mantle by subduction zones is only partly balanced by outward water transport by seafloor volcanism, and this imbalance represents a mechanism for sea level change. Here we have shown that dramatic changes in tectonic rates since the breakup of the last supercontinent (Figure 1) have induced changes in the overall efficiency of mantle regassing at subduction zones (Figures 4a and 4e). These fluctuations in regassing extend beyond fluctuations in the rate of convergence, which are always balanced by divergence at ridges. Therefore, it is unlikely that the present-day fluxes are representative for past and future fluxes, and the rate of sea level change that results from imbalanced degassing and regassing should change as the Earth's tectonic configuration changes. We find that even a present-day balance of the deep water fluxes implies a significant sea level drop over the last supercontinent cycle. A concise summary of our main findings reads as follows:

- By parameterizing the dependence of regassing efficiency (4) on plate age and velocity (through the thermal parameter), we can approximately recreate estimates of present-day water fluxes for subduction zones around the world (Figure 3). This allows us to extend present-day predictions of the subduction water flux to past times using plate kinematic models.
- By combining our reconstructed time history of degassing and regassing fluxes with previously published estimates for the present-day values of these fluxes, we can reconstruct the evolution of ocean water mass since 230 Ma. Our models predict a sea level drop (upper bound ~50 m) associated with deep water cycling even if regassing and degassing are currently balanced, and we consider amplitudes as large as ~130 m as possible if regassing currently dominates (Figure 4). Such amplitudes are comparable to those produced by other sea-level-changing mechanisms (Figure 7a) and can be accommodated within the sea level budget of the past 230 Myr without violating stratigraphic observations of sea level change (Figure 7b).
- We expect deep water fluxes to remain more or less stable during supercontinentality and for periods between dispersal and assembly. During supercontinent dispersal we expect a significant net flux of water from the oceans into the mantle caused by the opening of a new ridge system that forces rapid subduction

of old oceanic lithosphere. This period of faster sea level drop, happening repeatedly over several supercontinental cycles, may contribute significantly to the long-term regassing of the mantle that is thought to be an important part of Earth's thermal history.

Finally, looking ahead, we consider better constraints on the deep water fluxes for the present day, combined with more information about tectonic rates further back in time, essential for improving our understanding of the deep water cycle and its associated sea level change. Such advancements would represent important steps toward linking mantle dynamics and the exosphere and characterizing mantle water heterogeneity.

Appendix A: Monte Carlo Methods

The world uncertainty function (Figure A1a) is a measure of the Earth's present-day surface area fraction that is missing at a given point in time t and serves as a proxy for the uncertainty in any plate motion history model (Domeier & Torsvik, 2017). To capture this time-dependent uncertainty in our model results, we run a large number of simulations (10^4) for each model, and for each model run every tectonic input parameter (L_s, v_S, L_R, v_R, and τ) is multiplied by a perturbation factor p (the same factor is used for all segments within one model run to avoid unphysical discontinuities in, for example, spreading velocities along a mid-ocean ridge) that scales with the world uncertainty. Each perturbation factor is defined as $p_k = 1 + r_k W_N(t)$, where $k = 1, 2, .., 5$ and r_k is a random number drawn from the uncertainty distribution defined by $N(\mu, \sigma)$ with $\mu = 0$ and $2\sigma = W_{\max}$ (Figure A1b), $W_N(t)$ is the *normalized world uncertainty function* defined as $W_N(t) = W(t)/W_{\max}$, and $W_{\max} = 0.7$ is the maximum uncertainty (Figure A1a). We consider normal distributions around the original values because these values represent what the authors of the plate reconstructions model thought to be most plausible, and not just a random guess (which would be equivalent of assuming a uniform distribution). The equations for the perturbed tectonic parameters can then be expressed as:

$$\tilde{L_S} = p_1 L_s, \tag{A1}$$

$$\tilde{v_S} = p_2 v_s, \tag{A2}$$

$$\tilde{L_R} = p_3 L_R, \tag{A3}$$

$$\tilde{v_R} = p_4 v_R, \tag{A4}$$

$$\tilde{\tau} = p_5 \tau. \tag{A5}$$

To see the normally distributed variation in the tectonic parameters resulting from this sampling approach, see Figures 1f–1h. Because our model outputs are also distributions (however, they are nonnormal and nonsymmetric), rather than singles curves, we present the results as preferred estimates defined by the median, with upper and lower bounds defined by upper and lower quartile. The *upper quartile* and the *lower quartile* are defined as the median of the lower half of the distribution, while the upper bound is defined by the median of the upper half of the distribution (where the total median divides the distribution into halves); see Figure 4.

To ensure that the perturbations do not to violate the constant Earth surface condition, that is, divergence at mid-ocean ridges equals convergence at subduction zones $\sum \tilde{v_R} \tilde{L_R} = \sum \tilde{v_S} \tilde{L_S}$, the tectonic parameters must

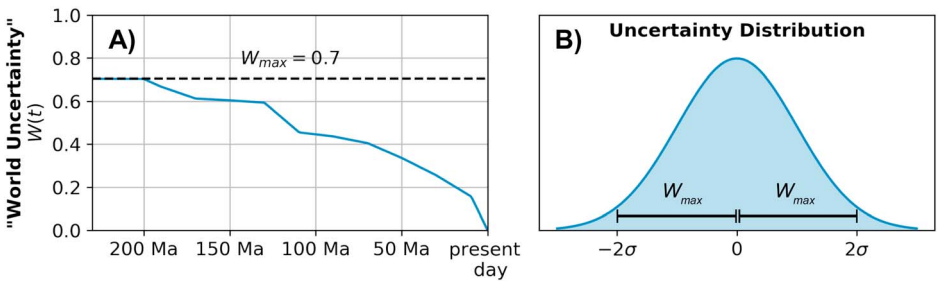

Figure A1. The fraction of Earth's present-day surface that is missing at a given point in time (a), and the assumed uncertainty in the tectonic parameters used in our models (b).

be sampled with care. Thus, the perturbation factors (p_1, p_2, p_3, p_4, and p_5) cannot be sampled completely independent of each other but are subject to the constraint $p_1 p_2 = p_3 p_4$. We solve this as follows:

1. Draw three random numbers r_1, r_2, r_5.
2. Compute p_1 and p_2 according to $p_i = 1 + r_i W_N(t)$.
3. Draw a binary number q with an equal chance of 1 and 0.
4. If $q = 0 \rightarrow p_3 = p_1$ and $p_4 = p_2$
   If $q = 1 \rightarrow p_3 = p_2$ and $p_4 = p_1$

The procedure above ensures that every perturbation (p_1, p_2, p_3, p_4, and p_5) remains normally distributed and proportional to the world uncertainty, while satisfying $p_1 p_2 = p_3 p_4$.

Acknowledgments
This paper has benefited from discussions with, and feedback from, several people. For valuable input on the time-dependent reliability of tectonic reconstructions, we thank Trond Torsvik and Mathew Domeier. All calculations (described in section 2 and Appendix A) were preformed using Python (Van Rossum & Drake, 1995). The input parameters from the tectonic reconstructions are available from Müller et al. (2016), and the other constants can be found in Table 1. The published model results used to calibrate the empirical law for deep water retention (equation (4) and Figures 3a and 3b) are available in van Keken et al. (2011) and Rüpke et al. (2004). We thank Fabio Crameri for the development of perceptually uniform and color-vision-deficiency friendly color maps (Crameri, 2018b), ensuring an accurate representation of the underlying data in the figures (Crameri, 2018a). Finally, we thank Adrian Lenardic, Jun Korenaga and one anonymous reviewer for insightful suggestions that greatly improved the manuscript. This work was funded by the Research Council of Norway's *Centres of Excellence Project 223272*.

References

Bodnar, R. J., Azbej, T., Becker, S. P., Cannatelli, C., Fall, A., & Severs, M. J. (2013). Whole Earth geohydrologic cycle, from the clouds to the core: The distribution of water in the dynamic Earth system. *The Geological Society of America Special Paper*, *500*, 431–61.

Cai, C., Wiens, D. A., Shen, W., & Eimer, M. (2018). Water input into the Mariana subduction zone estimated from ocean-bottom seismic data. *Nature*, *563*, 389–392.

Cloetingh, S., & Haq, B. U. (2015). Inherited landscapes and sea level change. *Science*, *347*(6220), 1258375.

Cogné, J.-P., & Humler, E. (2008). Global scale patterns of continental fragmentation: Wilson's cycles as a constraint for long-term sea-level changes. *Earth and Planetary Science Letters*, *273*(3-4), 251–259.

Conrad, C. P. (2013). The solid Earth's influence on sea level. *Geological Society of America Bulletin*, *125*(7-8), 1027–1052.

Conrad, C. P., & Husson, L. (2009). Influence of dynamic topography on sea level and its rate of change. *Lithosphere*, *1*(2), 110–120.

Conrad, C. P., Steinberger, B., & Torsvik, T. H. (2013). Stability of active mantle upwelling revealed by net characteristics of plate tectonics. *Nature*, *498*(7455), 479.

Crameri, F. (2018a). Geodynamic diagnostics, scientific visualisation and staglab 3.0. *Geoscientific Model Development*, *11*(6), 2541–2562.

Crameri, F. (2018b). Scientific colour-maps. Zenodo. http://doi.org/10.5281/zenodo.1243862

Crosby, A., & McKenzie, D. (2009). An analysis of young ocean depth, gravity and global residual topography. *Geophysical Journal International*, *178*, 1198–1219. https://doi.org/10.1111/j.1365-246X.2009.04224.x

Crowley, J. W., Gérault, M., & O'Connell, R. J. (2011). On the relative influence of heat and water transport on planetary dynamics. *Earth and Planetary Science Letters*, *310*(3), 380–388.

Domeier, M., & Torsvik, T. H. (2017). Full-plate modelling in pre-Jurassic time. *Geological Magazine*, *156*, 261–280.

Faccenda, M., Gerya, T. V., Mancktelow, N. S., & Moresi, L. (2012). Fluid flow during slab unbending and dehydration: Implications for intermediate-depth seismicity, slab weakening and deep water recycling. *Geochemistry, Geophysics, Geosystems*, *13*, Q01010. https://doi.org/10.1029/2011GC003860

Garrels, R. M. (1983). The carbonate-silicate geochemical cycle and its effect on atmospheric carbon dioxide over the past 100 million years. *American Journal of Science*, *283*, 641–683.

Hacker, B. R. (2008). H_2O subduction beyond arcs. *Geochemistry, Geophysics, Geosystems*, *9*, Q03001. https://doi.org/10.1029/2007GC001707

Hallam, A. (1992). *Phanerozoic sea-level changes*. New York: Columbia University Press.

Haq, B. U., Al-Qahtani, A. M. (2005). Phanerozoic cycles of sea-level change on the arabian platform. *GeoArabia*, *10*(2), 127–160.

Haq, B. U., & Schutter, S. R. (2008). A chronology of paleozoic sea-level changes. *Science*, *322*(5898), 64–68.

Hirschmann, M. (2006). Water, melting, and the deep Earth H_2O cycle. *Annual Review of Earth and Planetary Sciences*, *34*, 629–653.

Hirschmann, M. (2018). Comparative deep Earth volatile cycles: The case for C recycling from exosphere/mantle fractionation of major (H_2O, C, N) volatiles and from H_2O/Ce, CO_2/Ba, and CO_2/Nb exosphere ratios. *Earth and Planetary Science Letters*, *502*, 262–273.

Hirschmann, M. M., & Dasgupta, R. (2009). The h/c ratios of Earth's near-surface and deep reservoirs, and consequences for deep Earth volatile cycles. *Chemical Geology*, *262*(1-2), 4–16.

Hirschmann, M., & Kohlstedt, D. (2012). Water in Earth's mantle. *Physical Today*, *65*(3), 40.

Ito, E., Harris, D. M., & Anderson, A. T. Jr (1983). Alteration of oceanic crust and geologic cycling of chlorine and water. *Geochimica et Cosmochimica Acta*, *47*(9), 1613–1624.

Kasting, J. F., & Catling, D. (2003). Evolution of a habitable planet. *Annual Review of Astronomy and Astrophysics*, *41*(1), 429–463.

Kelemen, P. B., & Manning, C. E. (2015). Reevaluating carbon fluxes in subduction zones, what goes down, mostly comes up. *Proceedings of the National Academy of Sciences*, *112*, E3997–E4006.

Keller, T., Katz, R. F., & Hirschmann, M. (2017). Volatiles beneath mid-ocean ridges: Deep melting, channelised transport, focusing, and metasomatism. *Earth and Planetary Science Letters*, *464*, 55–68.

Kirby, S. H., Stein, S., Okal, E. A., & Rubie, D. C. (1996). Metastable mantle phase transformations and deep earthquakes in subducting oceanic lithosphere. *Reviews of geophysics*, *34*(2), 261–306.

Korenaga, J. (2007). Thermal cracking and the deep hydration of oceanic lithosphere: A key to the generation of plate tectonics? *Journal of Geophysical Research*, *112*, B05408. https://doi.org/10.1029/2006JB004502

Korenaga, J. (2008). Plate tectonics, flood basalts and the evolution of Earth's oceans. *Terra Nova*, *20*(6), 419–439.

Korenaga, J. (2011). Thermal evolution with a hydrating mantle and the initiation of plate tectonics in the early Earth. *Journal of Geophysical Research*, *116*, B12403. https://doi.org/10.1029/2011JB008410

Korenaga, J. (2013). Initiation and evolution of plate tectonics on Earth: Theories and observations. *Annual Review of Earth and Planetary Sciences*, *41*, 117–151.

Korenaga, J. (2017). On the extent of mantle hydration caused by plate bending. *Earth and Planetary Science Letters*, *457*, 1–9.

Korenaga, J., Planavsky, N. J., & Evans, D. A. (2017). Global water cycle and the coevolution of the Earth's interior and surface environment. *Philosophical Transactions of the Royal Society A*, *375*(2094), 20150393.

Li, Z.-X., & Zhong, S. (2009). Supercontinent–superplume coupling, true polar wander and plume mobility: Plate dominance in whole-mantle tectonics. *Physics of the Earth and Planetary Interiors*, *176*(3-4), 143–156.

Magni, V., Bouilhol, P., & van Hunen, J. (2014). Deep water recycling through time. *Geochemistry, Geophysics, Geosystems*, *15*, 4203–4216. https://doi.org/10.1002/2014GC005525

Marty, B., & Tolstikhin, I. N. (1998). CO_2 fluxes from mid-ocean ridges, arcs and plumes. *Chemical Geology*, *145*(3), 233–248.

Matthews, K. J., Maloney, K. T., Zahirovic, S., Williams, S. E., Seton, M., & Mueller, R. D. (2016). Global plate boundary evolution and kinematics since the late Paleozoic. *Global and Planetary Change*, *146*, 226–250.

Maunder, B., van Hunen, J., Bouilhol, P., & Magni, V. (2019). Modeling slab temperature: A reevaluation of the thermal parameter. *Geochemistry, Geophysics, Geosystems*, *20*, 673–687. https://doi.org/10.1029/2018GC007641

McGovern, P. J., & Schubert, G. (1989). Thermal evolution of the Earth: effects of volatile exchange between atmosphere and interior. *Earth and Planetary Science Letters*, *96*(1-2), 27–37.

Müller, R. D., Seton, M., Zahirovic, S., Williams, S. E., Matthews, K. J., Wright, N. M., et al. (2016). Ocean basin evolution and global-scale plate reorganization events since Pangea breakup. *Annual Review of Earth and Planetary Sciences*, *44*, 107–138.

Nance, R. D., Murphy, J. B., & Santosh, M. (2014). The supercontinent cycle: A retrospective essay. *Gondwana Research*, *25*(1), 4–29.

Nance, R. D., Worsley, T. R., & Moody, J. B. (1986). Post-Archean biogeochemical cycles and long-term episodicity in tectonic processes. *Geology*, *14*(6), 514–518.

Nestola, F., & Smyth, J. R. (2016). Diamonds and water in the deep Earth: A new scenario. *International Geology Review*, *58*(3), 263–276.

Parai, R., & Mukhopadhyay, S. (2012). How large is the subducted water flux? New constraints on mantle regassing rates. *Earth and Planetary Science Letters*, *317*, 396–406.

Parsons, B., & Sclater, J. G. (1977). An analysis of the variation of ocean floor bathymetry and heat flow with age. *Journal of geophysical research*, *82*(5), 803–827.

Peslier, A. H., Schönbächler, M., Busemann, H., & Karato, S.-I. (2017). Water in the Earth's interior: Distribution and origin. *Space Science Reviews*, *212*(1-2), 743–810.

Pitman, W. C. III (1978). Relationship between eustacy and stratigraphic sequences of passive margins. *Geological Society of America Bulletin*, *89*(9), 1389–1403.

Ranero, C. R., & Sallares, V. (2004). Geophysical evidence for hydration of the crust and mantle of the nazca plate during bending at the north chile trench. *Geology*, *32*(7), 549–552.

Rüpke, L. H., Morgan, J. P., Hort, M., & Connolly, J. A. (2004). Serpentine and the subduction zone water cycle. *Earth and Planetary Science Letters*, *223*(1-2), 17–34.

Sandu, C., Lenardic, A., & McGovern, P. (2011). The effects of deep water cycling on planetary thermal evolution. *Journal of Geophysical Research*, *116*, B12404. https://doi.org/10.1029/2011JB008405

Sclater, J., Jaupart, C., & Galson, D. (1980). The heat flow through oceanic and continental crust and the heat loss of the Earth. *Reviews of Geophysics*, *18*(1), 269–311.

Silver, P. G., & Behn, M. D. (2008). Intermittent plate tectonics? *Science*, *319*(5859), 85–88.

Straume, E., Gaina, C., Medvedev, S., Hochmuth, K., Gohl, K., Whittaker, J. M., et al. (2019). Globsed: Updated total sediment thickness in the world's oceans. *Geochemistry, Geophysics, Geosystems*, *20*, 1756–1772. https://doi.org/10.1029/2018GC008115

Syracuse, E. M., van Keken, P. E., & Abers, G. A. (2010). The global range of subduction zone thermal models. *Physics of the Earth and Planetary Interiors*, *183*(1-2), 73–90.

van Keken, P. E., Hacker, B. R., Syracuse, E. M., & Abers, G. A. (2011). Subduction factory: 4. Depth-dependent flux of H_2O from subducting slabs worldwide. *Journal of Geophysical Research*, *116*, B01401. https://doi.org/10.1029/2010JB007922

Van Rossum, G., & Drake, F. L. Jr (1995). *Python tutorial*. Netherlands: Centrum voor Wiskunde en Informatica Amsterdam.

Wegener, A. (1920). *Die entstehung der kontinente und ozeane* (Vol. 66). Berlin: F. Vieweg.

Worsley, T., Moody, J., & Nance, R. (1985). Proterozoic to recent tectonic tuning of biogeochemical cycles. *The carbon cycle and atmospheric CO2: natural variations Archean to present*, *32*, 561–572.

Worsley, T., Nance, R., & Moody, J. (1982). Plate tectonic episodicity: A deterministic model for periodic “pangeas”. *Eos, Transactions of the American Geophysical Union*, *65*(45), 1104.

Worsley, T. R., Nance, D., & Moody, J. B. (1984). Global tectonics and eustasy for the past 2 billion years. *Marine Geology*, *58*(3-4), 373–400.